

Thin superconductors and SQUIDs in perpendicular magnetic field

Ernst Helmut Brandt

Max-Planck-Institut für Metallforschung, D-70506 Stuttgart, Germany

(Dated: October 6, 2018)

It is shown how the static and dynamic electromagnetic properties can be calculated for thin flat superconducting films of any shape and size, also multiply connected as used for SQUIDs, and for any value of the effective magnetic London penetration depth Λ . As examples, the distributions of sheet current and magnetic field are obtained for rectangular and circular films without and with slits and holes, in response to an applied perpendicular magnetic field and to magnetic vortices moving in the film. The self energy and interaction of vortices with each other and with an applied magnetic field and/or transport current are given. Due to the long ranging magnetic stray field, these energies depend on the size and shape of the film and on the vortex position even in large films, in contrast to the situation in large bulk superconductors. The focussing of magnetic flux into the central hole of square films without and with a radial slit is compared.

PACS numbers: 74.78.-w, 74.25.Ha, 74.25.Op

I. INTRODUCTION

The calculation of the electromagnetic properties of thin superconducting films of finite size as used, e.g., in Superconducting Quantum Interference Devices (SQUIDs)¹ is a complicated problem since these sensitively depend on the shape and size of the film. This is so since the currents in thin films are not screened as in bulk superconductors, but interact via the magnetic stray field they generate outside the film. In particular, the self energy of a magnetic vortex in thin films (called Pearl vortex²) and the interaction between two such vortices depend on their position in the film even for very large films. This means a vortex is never “far from the film edges”, in contrast to the behavior of vortices in the bulk, whose energy, current density, and magnetic field become independent of the vortex position and of the specimen shape when the distance from the surface is much larger than the London penetration depth λ . This is so since in the bulk the factor $1/(1 + k_{\perp}^2 \lambda^2)$ in the Fourier transforms (with wave vector components $k_x, k_y, k_z, k_{\perp}^2 = k_x^2 + k_y^2$) causes the fields and currents to decay exponentially over the length λ at large distances from the vortex core. In thin films of thickness $d < \lambda$ the effective magnetic penetration depth $\Lambda = \lambda^2/d$ is larger than λ and the Fourier transforms contain a factor $1/(\frac{1}{2}k_{\perp} + k_{\perp}^2 \Lambda)$ that describes also the long-range non-exponential interaction of vortices via the magnetic stray field outside the film.

But even films in the ideal Meissner state containing no vortices present a difficult problem. Properties of macroscopic circular disks and rings in a perpendicular applied magnetic field were calculated recently for ideal screening ($\Lambda = 0$)³ and for arbitrary λ .⁴ When this ring has a radial slit, e.g. in a washer-shaped SQUID, the circular symmetry is lost, but some properties like the sheet current and the concentration of magnetic flux into the central hole (flux focussing) can still be calculated approximately from this circular symmetric model by forcing the current in the ring to be zero.^{3,4} (This situation may be achieved

by appropriate magnetic history.) Below we shall compare this approximation with the exact two-dimensional (2D) solution for a slitted ring and find partial agreement (Sec. III).

While the slitted ring or slitted square film with an applied magnetic field H_a and/or transport current I_a are simply connected geometries (Fig. 1, right two plots), a closed ring or a slitted film with the entrance of the slit short-cut by superconducting contacts (e.g. by weak links) present multiply connected geometries (Fig. 1, left two plots). These are more difficult to calculate since the (quantized) magnetic flux Φ (or fluxoid Φ_f when $\Lambda > 0$) trapped in this hole, and the current I circulating around the hole, are additional parameters, besides H_a and I_a . In films with n holes or slots that are fully surrounded by superconducting material, there are n such fluxoids Φ_{fi} and currents I_i that depend on the magnetic history and that may be used to define n self-inductances $L_i = \Phi_{fi}/I_i$ and $n(n-1)/2$ mutual inductances $M_{ij} = \Phi_{fi}/I_j$.

This paper shows how all these (actually 3D) thin-film problems can be solved numerically by a 2D matrix inversion method allowing for non-equidistant grid points. The presented general equations and concrete examples generalize previous methods that either work only for equidistant spatial grids⁵ (which are not very accurate near the film edges or near a narrow slit or small hole), or for general grid did not account for finite penetration depth $\Lambda > 0$,⁶ or assumed simply connected geometry,^{5,6} or applied only to circular disks or rings.^{3,4} In this paper I consider the electrodynamics of finite-sized macroscopic films that can be described by London theory, which applies when the magnetic field is much smaller than the upper critical field H_{c2} and the superconductor is much larger than the coherence length ξ . The application to SQUIDs will be dealt with elsewhere.⁷ In the present paper I shall thus not need the notions of fluxoid quantization, phase of the superconducting order parameter, vector potential, and voltages caused by the Josephson effect, but some quantities computed here will be needed in the theory of SQUIDs, e.g., self-inductance and effec-

tive area.

Our 2D matrix inversion method can be quite accurate even when the number of grid points is not very large. For example, in the ideal Meissner state with $\Lambda = 0$, the computed current density exactly yields $H_z(x, y, 0) = 0$ inside the film ($z = 0$ is the film plane). For $\Lambda > 0$, accurate results are obtained even when Λ is smaller than the spacing of our rectangular grid. For similar calculations using a finite-element method and a different integral kernel (or matrix) see Ref. 8. Analytical^{4,9} and numerical¹⁰ London calculations were performed in the limit of large Λ , i.e., for small disks with radius $R \ll \Lambda$. (Here I shall not list numerous recent work on mesoscopically small superconductors with vortices computed from Ginzburg-Landau theory.) An elegant and fast method that computes the currents in films from the magnetic field pattern measured at the film surface with high resolution, without having to store or explicitly invert a large matrix, is described by Wijngaarden et al.;^{11,12} this method has all advantages of the direct matrix inversion method and avoids the inversion by Fourier transform, that would require knowledge of the magnetic field pattern also outside the film area. The static Bean model for thin films of any shape is computed by Prigozhin using a variational method.¹³

II. CALCULATION METHOD

This section describes how for thin flat superconducting films of any shape, also multiply connected as needed for SQUIDS, one can calculate the static and dynamic response to an applied magnetic field, applied electric current, and to vortices moving in the film. In such problems the central physical quantity is the thickness-integrated current density, called sheet current $\mathbf{J}(x, y) = \int dz \mathbf{j}(x, y, z) = (J_x, J_y)$. For films with constant thickness d and nearly z -independent current density $\mathbf{j}(x, y, z)$ one approximately has $\mathbf{J} = \mathbf{j}d$, but the following equations are more general, applying also to films with spatially varying thickness $d(x, y)$ if the typical length of this variation is $\gg d$.

A. Properties of the stream function

Since one has $\nabla \cdot \mathbf{J} = 0$ in the film except at small contacts, one can express \mathbf{J} in terms of a scalar potential or stream function $g(x, y)$ as $\mathbf{J} = -\hat{\mathbf{z}} \times \nabla g = \nabla \times (\hat{\mathbf{z}}g) = (\partial g / \partial y, -\partial g / \partial x)$. The function $g(x, y)$ has several useful properties and interpretations:

1. $g(x, y)$ is the local magnetization or density of tiny current loops.
2. The contour lines of $g(x, y)$ are the current stream lines. Typical $g(x, y)$ look like a mountain (Fig. 2).
3. On the boundary of the film one may put $g(x, y) = 0$ since the boundary coincides with a stream line.

4. The integral of $g(x, y)$ over the film area equals the magnetic moment of the film if $g = 0$ on its edge.

5. The difference $g(\mathbf{r}_1) - g(\mathbf{r}_2)$ is the current that crosses any line connecting the two points \mathbf{r}_1 and \mathbf{r}_2 .

6. If the film contains an isolated hole or slot such that magnetic flux can be trapped in it or a current I can circulate around it, then in this hole one has $g(x, y) = \text{const} = I$ if $g(x, y) = 0$ is chosen outside the film.

7. In a multiply connected film with n holes, n independent constants $g_1 \dots g_n$ can be chosen for the values of $g(x, y)$ in each of these holes. The current flowing between hole 1 and hole 2 is then $g_1 - g_2$.

8. A vortex with flux Φ_0 in the film moves in the potential $V = -\Phi_0 g(x, y)$, since the Lorentz force on a vortex is $-\mathbf{J} \times \hat{\mathbf{z}}\Phi_0 = -\Phi_0 \hat{\mathbf{z}} \times (\hat{\mathbf{z}} \times \nabla g) = \Phi_0 \nabla g(x, y) = -\nabla V$.

9. A vortex moving from the edge of the film into a hole connected to the outside by a slit, at each position (x, y) couples a fluxoid $g(x, y)\Phi_0/I$ into this hole, where $g(x, y)$ is the solution that has $g(x, y) = I$ in this hole (with closed slit, see point 6) and $g = 0$ outside the film.

10. When the film has n holes, a vortex in the film at (x, y) couples a fluxoid $g_i(x, y)\Phi_0/I$ into the i th hole (if this is connected to the edge by a slit), where $g_i(x, y)$ is the solution exhibiting $g_i = I$ in this hole and $g_i = 0$ in all other (isolated) holes and on the film edge.

B. Ampère's law for thin films

From Ampère's local 3D law $\mathbf{j} = \nabla \times \mathbf{H}$ one obtains for a current-carrying film in the plane $z = 0$ a nonlocal 2D relation between the perpendicular magnetic field $H_z(x, y, 0)$ and the stream function $g(x, y)$:

$$H_z(\mathbf{r}) = H_a(\mathbf{r}) + \int_S d^2r' Q(\mathbf{r}, \mathbf{r}') g(\mathbf{r}'). \quad (1)$$

Here $\mathbf{r} = (x, y)$, $H_a(\mathbf{r})$ is the z component of the applied magnetic field, and S is the area of the film. The integral kernel $Q(\mathbf{r}, \mathbf{r}')$ has the meaning of the magnetic field (along z) caused at point \mathbf{r} in the plane of the film by a magnetic dipole (or tiny current loop) of unit strength positioned at \mathbf{r}' and directed along z . From the known dipole field in any plane $z = \text{const}$, one obtains formally:

$$Q(\mathbf{r}, \mathbf{r}') = Q(\rho) = \lim_{z \rightarrow 0} \frac{2z^2 - \rho^2}{4\pi(z^2 + \rho^2)^{5/2}}. \quad (2)$$

Note that this kernel depends only on the distance $\rho = |\mathbf{r} - \mathbf{r}'|$. For $\rho \neq 0$ one has $Q(\rho) = -1/(4\pi\rho^3)$, but the integral of $Q(\rho)$ over the infinite plane vanishes, i.e., the total magnetic flux of a dipole is zero in any plane $z = \text{const}$, also for $z \rightarrow 0$, thus $Q(\rho)$ is *highly singular* at $\rho = 0$. For explicit calculations one has to decide how to deal with this singularity of Q .

For numerics, one has to write the integral as a sum. Defining a 2D grid whose N points \mathbf{r}_i fill the film area S ,

one may approximate any integral over S by a sum,

$$\int_S d^2r f(\mathbf{r}) \approx \sum_{i=1}^N w_i f(\mathbf{r}_i), \quad (3)$$

where the w_i are weights, e.g., $w_i = \text{const} = S/N$ for equidistant grids that avoid the film edges, see Appendix A. The accuracy of this numerical integration can be strongly increased by choosing an appropriate non-equidistant grid, e.g., a grid that is denser near the boundary of S or near possible poles or jumps of the integrand $f(x, y)$. Equation (1) now becomes

$$H_z(\mathbf{r}_i) = H_a(\mathbf{r}_i) + \sum_j Q_{ij} w_j g(\mathbf{r}_j) \quad (4)$$

with the matrix $Q_{ij} = Q(\mathbf{r}_i, \mathbf{r}_j)$. Equation (4) is formally solved by matrix inversion, i.e., by writing

$$g(\mathbf{r}_i) = \sum_j K_{ij} [H_z(\mathbf{r}_j) - H_a(\mathbf{r}_j)], \quad (5)$$

where K_{ij} is the inverse matrix

$$K_{ij} = (Q_{ij} w_j)^{-1} \quad (6)$$

defined by the equation $\sum_l K_{il} (Q_{lj} w_j) = \delta_{ij}$ with $\delta_{ij} = 1$ for $i = j$ and $\delta_{ij} = 0$ for $i \neq j$. Note that, in contrast to Q_{ij} , the inverse matrix K_{ij} depends on the shape of the film and not only on the difference $\mathbf{r}_i - \mathbf{r}_j$. For the film shapes we have tested, all the matrix elements K_{ij} are found to be negative, with a sharp negative peak at $i = j$, and tending to zero when \mathbf{r}_i or \mathbf{r}_j approaches the film edge, see Fig. 3 for an example. In principle, the inverse kernel $K(x, y; x', y')$, integrated over y and y' (the strip width) was introduced¹⁴ and depicted¹⁵ earlier in the context of the magnetostatic energy of a tilted and curved narrow superconducting strip with pinned vortices. Then, and later,¹⁶ $K(x, y; x', y')$ was calculated by iterating an integral equation.

A useful expression for the matrix Q_{ij} was obtained in terms of a Fourier series in Ref. 5, but this method works only for equidistant grids, while for non-equidistant grids the matrix inversion is singular. This numerical form of Q_{ij} is thus not very accurate when one is interested in the sharply peaked \mathbf{J} and H_z near the film edges, or when the film exhibits fine structures, e.g., a small hole or narrow slit, since the maximum number of grid points on present Personal Computers is limited to about $N = 5000$, yielding a very large $N \times N$ matrix Q_{ij} .

A matrix Q_{ij} that works well for any grid \mathbf{r}_i , also with non-constant weights w_i , is obtained as follows. From Eq. (2) one has for $i \neq j$:

$$Q_{i \neq j} = -\frac{1}{4\pi |\mathbf{r}_i - \mathbf{r}_j|^3} = -q_{ij}. \quad (7)$$

The diagonal terms Q_{ii} are obtained from the condition that the integral of $Q(\rho)$ taken over the infinite area has

to vanish. Splitting this integral into the integral over the film area S plus the integral over the infinite area \bar{S} outside S , and writing the first integral as a sum, we get:

$$\begin{aligned} 0 &= \int_{\infty} d^2r' Q(\mathbf{r}_i - \mathbf{r}') \\ &\approx \sum_j Q_{ij} w_j + \int_{\bar{S}} d^2r' Q(\mathbf{r}_i - \mathbf{r}'). \end{aligned} \quad (8)$$

Defining a 2D function $C(\mathbf{r})$ as an integral over the film area or as a contour integral over the film edge,

$$C(\mathbf{r}) = \int_{\bar{S}} \frac{d^2r'}{4\pi |\mathbf{r} - \mathbf{r}'|^3} = \int_0^{2\pi} \frac{d\phi}{4\pi R(\phi)} \quad (9)$$

with $R = |\mathbf{r} - \mathbf{r}'|$ (ϕ is the angle between the vector $\mathbf{R} = \mathbf{r} - \mathbf{r}'$ pointing to the point \mathbf{r}' on the film edge and any fixed direction, say, the $+x$ axis), and writing $C_i = C(\mathbf{r}_i)$, $q_{ij} = 1/(4\pi |\mathbf{r}_i - \mathbf{r}_j|^3)$, we get from (8) the diagonal term $Q_{ii} w_i = \sum_{j \neq i} q_{ij} w_j + C_i$. The full matrix reads thus:

$$Q_{ij} = (\delta_{ij} - 1) q_{ij} + \delta_{ij} \left(\sum_{l \neq i} q_{il} w_l + C_i \right) / w_j. \quad (10)$$

Note that the terms in (10) should not be rearranged since $q_{ii} = \infty$. The matrix (10) is well behaved during inversion, so one may write

$$K_{ij} = \left[(\delta_{ij} - 1) q_{ij} w_j + \delta_{ij} \left(\sum_{l \neq i} q_{il} w_l + C_i \right) \right]^{-1}. \quad (11)$$

For a rectangular film filling the area $|x| \leq a$, $|y| \leq b$ one has explicitly from Eq. (9):^{5,16}

$$C(x, y) = \frac{1}{4\pi} \sum_{p, q} \left[(a - px)^{-2} + (b - qy)^{-2} \right]^{1/2} \quad (12)$$

with $p, q = \pm 1$. Interestingly, expression (12) may be used also for films that have a hole or slit, or several holes, or that do not fill the rectangle completely, e.g., a circular disk with radius $\leq a = b$. In such cases one has to omit in Eq. (4) and (5) the grid points that fall outside the film (but keep the points in isolated holes, see Sect. II E). Therefore, Eq. (5) with the explicit kernel K_{ij} from Eq. (11) and C_i from Eq. (12), allows one to compute the stream function $g(x, y)$ and thus the sheet current for thin films of arbitrary shape when one knows the magnetic field $H_z(x, y) - H_a(x, y)$ generated inside the film by this current. Information on H_z outside the film is *not* required for this stable inversion method.

C. Static solution of London equation

In superconductor films with thickness $d < \lambda$, the London penetration depth, the 3D static London equation

$\lambda^2 \nabla \times \mathbf{j} + \mathbf{H} = 0$ may be integrated over the film thickness d to yield the 2D equation

$$H_z(x, y) = -\Lambda[\nabla \times \mathbf{J}(x, y)] \cdot \hat{\mathbf{z}} = \Lambda \nabla^2 g(x, y), \quad (13)$$

where $\Lambda = \lambda^2/d$ is the effective London depth of the film. Eliminating $H_z(x, y)$ from Eqs. (1) and (13) one obtains an implicit equation for $g(x, y)$:

$$\begin{aligned} H_a(\mathbf{r}) &= - \int_S d^2 r' Q(\mathbf{r}, \mathbf{r}') g(\mathbf{r}') + \Lambda \nabla^2 g(\mathbf{r}) \\ &= - \int_S d^2 r' [Q(\mathbf{r}, \mathbf{r}') - \delta(\mathbf{r} - \mathbf{r}') \Lambda \nabla^2] g(\mathbf{r}') \end{aligned} \quad (14)$$

or with the discretized Eq. (4),

$$H_a(\mathbf{r}_i) = - \sum_j (Q_{ij} w_j - \Lambda \nabla_{ij}^2) g(\mathbf{r}_j). \quad (15)$$

In it the matrix ∇_{ij}^2 computes the Laplacean $\nabla^2 = \partial^2/\partial x^2 + \partial^2/\partial y^2$ at $\mathbf{r} = \mathbf{r}_i$ of a function defined on a grid, e.g., from the values $g(\mathbf{r}_j)$ at $\mathbf{r}_j = \mathbf{r}_i$ and its four nearest neighbors. Equation (15) is solved for $g(x, y)$ by matrix inversion:

$$g(\mathbf{r}_i) = - \sum_j K_{ij}^\Lambda H_a(\mathbf{r}_j) \quad (16)$$

with the inverse matrix

$$K_{ij}^\Lambda = (Q_{ij} w_j - \Lambda \nabla_{ij}^2)^{-1} \quad (17)$$

now depending on Λ . This matrix inversion is the more stable the larger is Λ , since finite Λ increases the diagonal terms and makes the resulting K_{ij}^Λ a smoother function as compared to the case $\Lambda = 0$ considered in Eq. (6). Examples for $H_z(x, y)$ are shown in Fig. 4 for a square with slit and hole, while Fig. 5 shows some profiles $H_z(x, 0)$ along the y -axis for the same square. Note that even small $\Lambda = 0.01a$ allows H_z to partly penetrate the entire film.

D. Dynamic solution of London equation

The time dependent behavior of superconducting films containing vortices may be described within continuum theory by the following realistic relation between the local electric field $\mathbf{E}(x, y, t)$ and the sheet current \mathbf{J} and magnetic induction $\mathbf{B} = \mu_0 \mathbf{H}$:⁵

$$\mathbf{E} = \rho_s(J, B) \mathbf{J}(\mathbf{r}, t) + \mu_0 \Lambda \dot{\mathbf{J}}(\mathbf{r}, t). \quad (18)$$

Here $\rho_s = \rho/d$ is the sheet resistivity caused by moving vortices, and the second term with $\Lambda = \lambda^2/d$ and $\dot{\mathbf{J}} = \partial \mathbf{J} / \partial t$ is the London term describing acceleration of Cooper pairs. The isotropic model (18) assumes that the resistivity ρ depends only on the magnitudes J and B . For example, without vortex pinning and Hall effect, one has free flux flow with $\rho = \rho_{\text{FF}} \approx (B/B_{c2}) \rho_n$, where ρ_n

is the resistivity in the normal conducting state and B_{c2} is the upper critical field. For thermally activated depinning a realistic model is $\rho = \rho_0 |J/J_c(B)|^\sigma$ with creep exponent $\sigma \gg 1$ and an in general B dependent critical sheet current $J_c(B)$. For a generalization to anisotropic superconductors see Ref. 5.

From the induction law $\dot{\mathbf{B}} = -\nabla \times \mathbf{E}$, which in the film plane reduces to $\dot{B}_z = \partial E_x / \partial y - \partial E_y / \partial x$, and from $\mathbf{J} = -\hat{\mathbf{z}} \times \nabla g$, one obtains $\mu_0 \dot{H}_z = \dot{B}_z = \nabla[\rho_s \nabla g] + \mu_0 \Lambda \nabla^2 \dot{g}$. Inserting this into the time derivative of Eq. (1) one finds an equation for $g(\mathbf{r}, t)$:

$$\begin{aligned} \int_S d^2 r' [Q(\mathbf{r}, \mathbf{r}') - \delta(\mathbf{r} - \mathbf{r}') \Lambda \nabla^2] \dot{g}(\mathbf{r}', t) \\ = f(\mathbf{r}, t) - \dot{H}_a(\mathbf{r}, t), \\ f(\mathbf{r}, t) = \mu_0^{-1} \nabla[\rho_s(\mathbf{r}, t) \nabla g(\mathbf{r}, t)]. \end{aligned} \quad (19)$$

In discretized form this becomes [cf. Eq. (15)]:

$$\sum_j (Q_{ij} w_j - \Lambda \nabla_{ij}^2) \dot{g}(\mathbf{r}_j) = f(\mathbf{r}_i, t) - \dot{H}_a(\mathbf{r}_i, t). \quad (20)$$

Inverting this one obtains the equation of motion for $g(x, y, t)$ in explicit form:

$$\dot{g}(\mathbf{r}_i, t) = \sum_j K_{ij}^\Lambda [f(\mathbf{r}_j, t) - \dot{H}_a(\mathbf{r}_j, t)] \quad (21)$$

with K_{ij}^Λ from Eq. (17). In the Meissner state or for rigidly pinned vortices one has $\rho_s = 0$ and these dynamic equations reduce to the static equations of Sect. II C.

E. Multiply connected films

Multiply connected films have one or more holes or slots that are completely surrounded by superconducting material and thus can trap magnetic flux. As a fundamental example I consider here a film containing one such hole with flux trapped such that a current I circulates around the hole when no magnetic field is applied, $H_a = 0$. In this case one has $g(x, y) = 0$ outside the film and $g(x, y) = I$ in the hole, and inside the film $g(x, y)$ smoothly goes from 0 to I . Generalization of this example to the presence of more holes and to $H_a \neq 0$ is possible by linear superposition.

This problem may be solved in three steps. First, consider the situation where $g = I$ in the hole and $g = 0$ everywhere outside the hole. This means a sharply localized sheet current of size I flows along the edge of the hole where this $g(x, y)$ has a jump. Such an edge current formally can be caused by an effective applied field

$$H_a^{\text{eff}}(\mathbf{r}_i) = -I \sum_{j \text{ in hole}} (Q_{ij} w_j - \Lambda \nabla_{ij}^2), \quad (22)$$

cf. Eq. (15). Next the real sheet current in the film is found as the $\mathbf{J} = -\hat{\mathbf{z}} \times \nabla g$ that generates this $H_a^{\text{eff}}(\mathbf{r})$

inside the film, cf. Eq. (16):

$$\begin{aligned} g(\mathbf{r}_i) &= - \sum_{j \text{ in film}} K_{ij}^\Lambda H_a^{\text{eff}}(\mathbf{r}_j) & \text{for } \mathbf{r}_i \text{ in the film,} \\ g(\mathbf{r}_i) &= I & \text{for } \mathbf{r}_i \text{ in the hole,} \\ g(\mathbf{r}) &= 0 & \text{outside the film.} \end{aligned} \quad (23)$$

Finally, the real magnetic field in the entire plane $z = 0$ is obtained as the field caused by this current, cf. Eq. (4):

$$H_z(\mathbf{r}_i) = \sum_j Q_{ij} w_j g(\mathbf{r}_j), \quad (24)$$

where now the sum is over all \mathbf{r}_j in the film and in the hole. This method works for any value of Λ and yields continuous functions $g(x, y)$ and $H_z(x, y)$ when $\Lambda > 0$. When $\Lambda = 0$ (ideal screening) the resulting $H_z(x, y)$ has sharp jumps at the film edges since in that case H_z exactly vanishes inside the film and has sharp infinities just outside the film edges (also in the hole), where $H_z \propto \delta^{-1/2}$ (δ is the distance from the edge). The current density in the film for $\Lambda = 0$ diverges similarly, but on the inner side of the edges, where $g \propto \delta^{1/2}$ and $J \propto \delta^{-1/2}$. For $\Lambda > 0$ the sheet current at the edges is finite and the infinities of H_z are logarithmic on both sides of all edges.

F. Individual vortices in the film

The sheet current, magnetic field, and energy of vortices in the film is obtained by linear superposition from the solution for one vortex and the interaction energy of a vortex pair. In a film of finite size all these results explicitly depend on the vortex positions and not only on their distances due to the strong effect of the film edges. The existence of one vortex at position \mathbf{r}_v modifies the static London Equation of Sect. II C to give $\lambda^2 \nabla \times \mathbf{j} + \mathbf{H} = (\Phi_0/\mu_0) \hat{\mathbf{z}} \delta_2(\mathbf{r} - \mathbf{r}_v)$, where $\Phi_0 = h/2e = 2.07 \cdot 10^{-15} \text{ Tm}^2$ is the quantum of flux and $\delta_2(\mathbf{r})$ is the 2D delta function. Equations (13) and (14) then become

$$H_z(\mathbf{r}) - \Lambda \nabla^2 g(\mathbf{r}) = \mu_0^{-1} \Phi_0 \delta_2(\mathbf{r} - \mathbf{r}_v), \quad (25)$$

$$\begin{aligned} \int_S d^2 r' [Q(\mathbf{r}, \mathbf{r}') - \delta(\mathbf{r} - \mathbf{r}') \Lambda \nabla^2] g(\mathbf{r}') \\ = \mu_0^{-1} \Phi_0 \delta_2(\mathbf{r} - \mathbf{r}_v) - H_a(\mathbf{r}). \end{aligned} \quad (26)$$

Writing the integral as a sum yields

$$\begin{aligned} \sum_j (Q_{ij} w_j - \Lambda \nabla_{ij}^2) g(\mathbf{r}_j) \\ = \mu_0^{-1} \Phi_0 \delta_2(\mathbf{r}_i - \mathbf{r}_v) - H_a(\mathbf{r}_i). \end{aligned} \quad (27)$$

To invert this and find $g(\mathbf{r}_i)$ and the vortex interaction, we have to assume that the vortex sits on a grid point, $\mathbf{r}_v = \mathbf{r}_j$. Averaging over the grid cell centered at \mathbf{r}_j and having an area w_j , replaces $\delta_2(\mathbf{r}_i - \mathbf{r}_j)$ by δ_{ij}/w_j . Inverting this and performing the sum containing δ_{ij} then

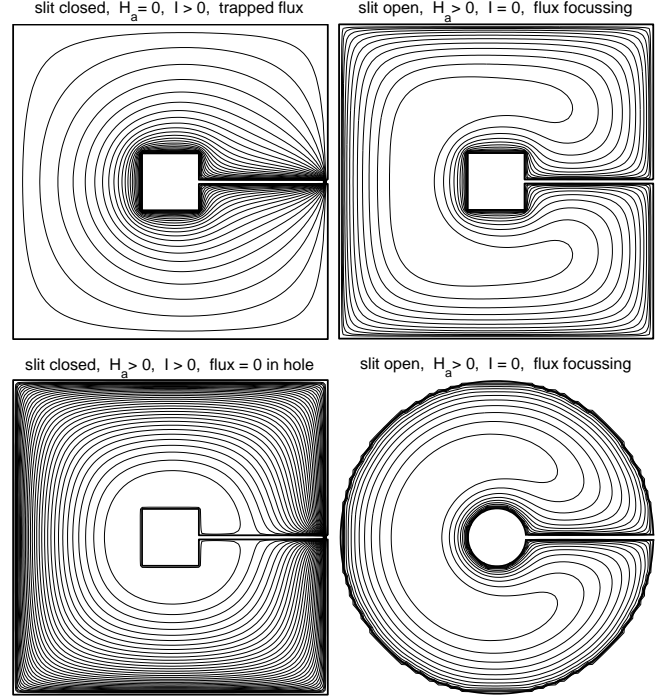


FIG. 1: Current stream lines in a thin film square with square hole and radial slit, and in a circular disk with circular hole and slit, in the ideal Meissner state $\Lambda = 0$. Top left: Slit bridged at the edge, circulating current $I > 0$ flows due to flux trapped in the hole and slit, no applied field $H_a = 0$. Top right and bottom right: Slit open, applied field $H_a > 0$, magnetic flux enters the slit and is focussed into the hole where $H(x, y) > H_a$. Bottom left: Closed slit, applied field $H_a > 0$, some current $I > 0$ flows such that the flux in hole and slit is exactly zero (ideal screening); this state is a superposition of the two upper states. Note that the current near the hole circulates in opposite direction, except in the trapped-flux case.

yields the stream function caused by a vortex positioned at \mathbf{r}_j and by the applied field $H_a(\mathbf{r}_i)$:

$$g(\mathbf{r}_i) = \mu_0^{-1} \Phi_0 K_{ij}^\Lambda / w_j - \sum_l K_{il}^\Lambda H_a(\mathbf{r}_l) \quad (28)$$

with the inverse matrix K_{ij} from Eq. (17), see also Eq. (16).

A second vortex sitting at \mathbf{r}_i sees the potential $-\Phi_0 g(\mathbf{r}_i)$; the interaction energy between two vortices positioned at \mathbf{r}_i and \mathbf{r}_j is thus:

$$V(\mathbf{r}_i, \mathbf{r}_j) = V_{ij} = V_{ji} = -\mu_0^{-1} \Phi_0^2 K_{ij}^\Lambda / w_j. \quad (29)$$

This potential is repulsive (positive) and sharply peaked at $\mathbf{r}_i = \mathbf{r}_j$, since all the K_{ij}^Λ are negative. One can show that the matrix K_{ij}^Λ / w_j is indeed symmetric in i, j , $K_{ij}^\Lambda / w_j = K_{ji}^\Lambda / w_i$. For $\Lambda = 0$ this is directly seen from the definition, Eq. (6), writing $\delta_{ij} = \sum_l K_{il} (Q_{lj} w_j) = \sum_l (K_{il} / w_l) (w_l Q_{lj} w_j)$, which shows that K_{il} / w_l is the inverse of the symmetric matrix $w_l Q_{lj} w_j$ and is thus sym-

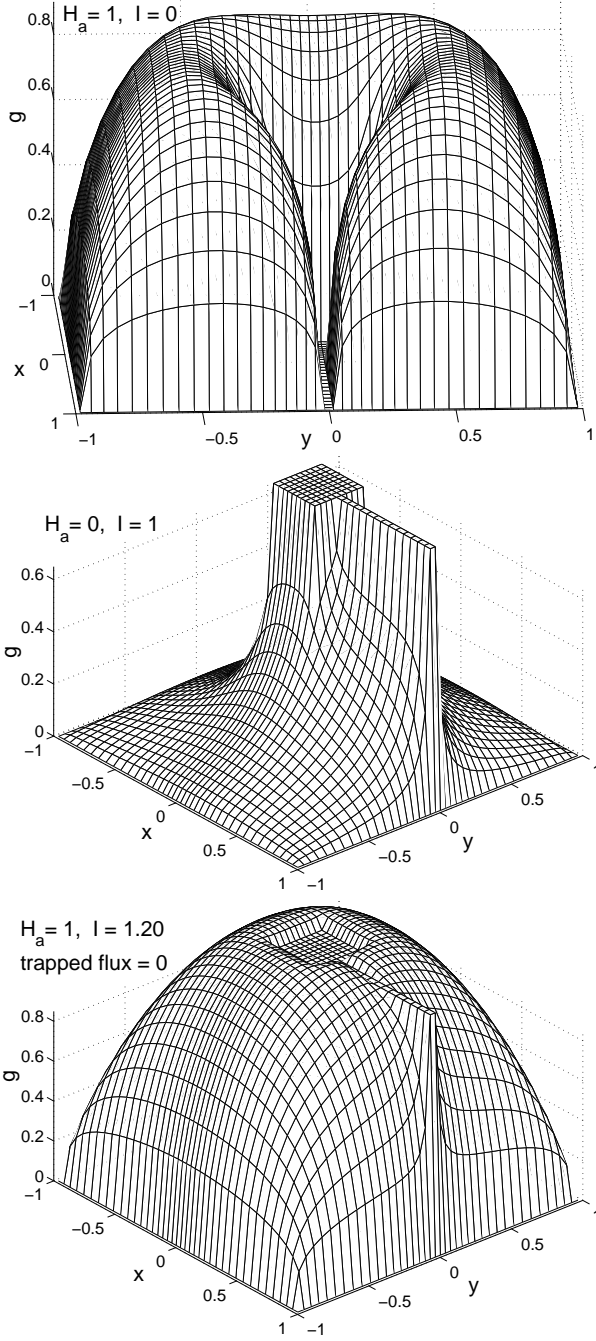


FIG. 2: The three examples of Fig. 1 for the stream function $g(x, y)$ in a square film (size 2×2 in units of half width a) with square hole (half width $a_1 = 0.2a$) and open slit (width $0.04a$), for 40×40 grid points, as Fig. 3. For penetration depth $\Lambda = 0$ (ideal screening). At the film edges $g(x, y)$ goes to zero with vertical slope, and outside the film $g = 0$ (for $\Lambda > 0$, the slope of g at the edges is finite, equal to the sheet current). Top: Constant applied field $H_a = 1$, open slit meaning a current $I = 0$, thus $g = 0$ in slit and hole (like Fig. 1 top right). Middle: $H_a = 0$, current $I = 1$ flowing around the hole and closed slit due to trapped flux, yielding $g = 1$ in hole and slit (like Fig. 1 top left). Bottom: Top and middle cases superimposed such that the flux trapped in the hole and slit is zero (like Fig. 1 bottom left): weights 1 and 1.2, thus in slit and hole $g = I = 1.2aH_a$.

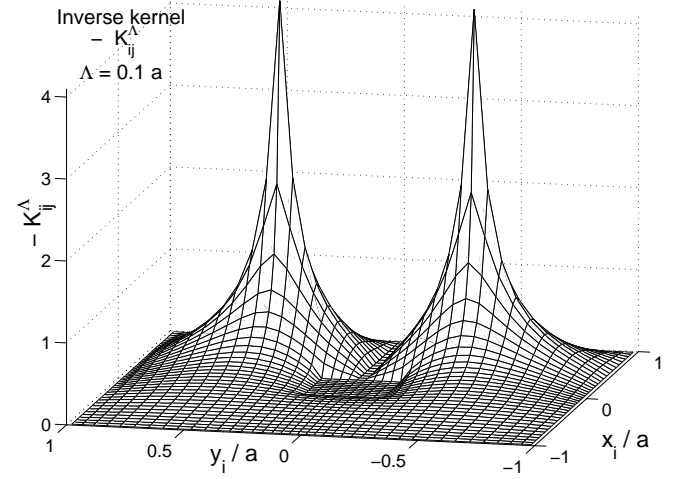


FIG. 3: Example for the inverse matrix $K_{ij}^\Lambda = K^\Lambda(\mathbf{r}_i, \mathbf{r}_j)$ in a square film (half width a) with square hole (half width $a_1 = 0.2a$) and open slit (width $0.04a$), similar to the squares in Figs. 1 and Fig. 2. For 40×40 grid points \mathbf{r}_i and constant $\mathbf{r}_j = (0.48, 0.42)a$, penetration depth $\Lambda = 0.1a$. At the film edges and in hole and slit one has $K_{ij}^\Lambda = 0$. The plotted K_{ij}^Λ is approximately symmetric in i, j since here the weights $w_i \approx \text{const}$. It also shows the interaction between a vortex at (x, y) and a vortex pair (due to the imposed symmetry) sitting at $(x_j, y_j) = (0.48, \pm 0.42)a$, cf. Eq. (29). Its contours are the current stream lines of this vortex pair. For $\Lambda = 0$, $K_{ij}^\Lambda = K_{ij}$ looks similar, but the peak is higher and the slopes at the edges are vertical.

metric itself. For $\Lambda > 0$ one also has to prove that the operator ∇_{ij}/w_j is symmetric, see Appendix.

When the film contains several vortices positioned at some of the grid points \mathbf{r}_j , then the sum over these \mathbf{r}_j has to be performed in the first term of Eq. (28), and the total energy of this vortex system becomes:

$$\begin{aligned}
 F &= \sum_i F_s(\mathbf{r}_i) + \sum_{j>i} V_{ij} + \sum_i V_a(\mathbf{r}_i) \\
 &\approx \frac{1}{2} \sum_{j,i} V_{ij} + \sum_i V_a(\mathbf{r}_i), \quad (30)
 \end{aligned}$$

where the sums are over the vortex positions i, j , $F_s(\mathbf{r}_i) \approx \frac{1}{2}V_{ii}$ is the self energy of the vortex, V_{ij} is the vortex interaction (29), and $V_a(\mathbf{r}_i) = \sum_l K_{il}^\Lambda H_a(\mathbf{r}_l)$ is the potential caused by the applied field $H_a(\mathbf{r})$. For constant H_a the external potential $V_a(\mathbf{r}_i) = H_a \sum_l K_{il}^\Lambda$ has the shape of a negative trough which is zero along the film edges. The vortices are thus pulled into the film by this potential.

G. Self energy of a vortex in the film

In contrast to vortices in large bulk superconductors, the self energy of a vortex in a thin film depends on the film size and shape and on the vortex position even when it is far from the film edges. Calculating this vortex energy from the 2D current density in the film and

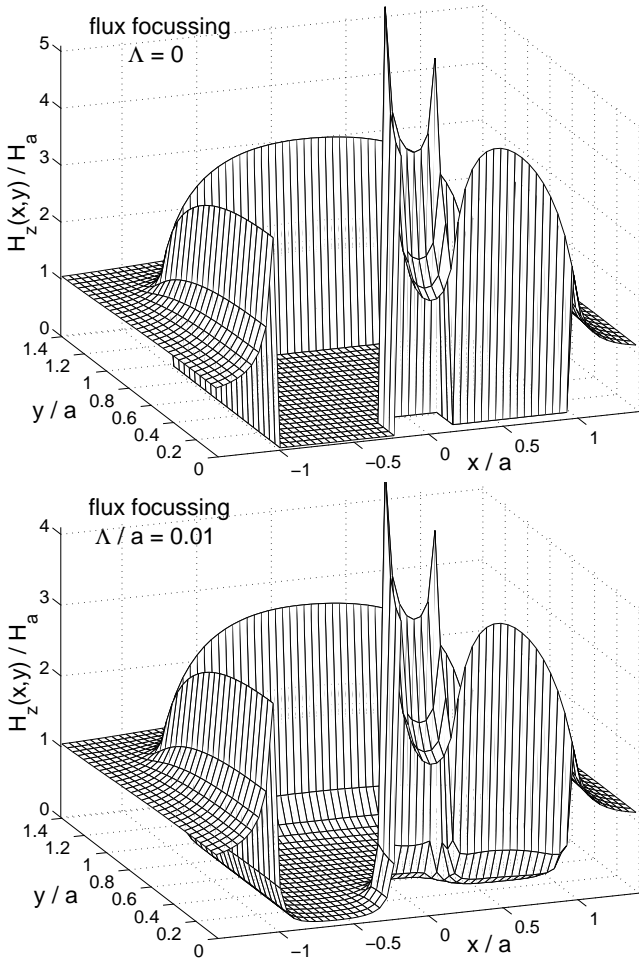


FIG. 4: The magnetic field $H_z(x, y)$ in the plane of a thin square with hole and slit, $H_a > 0$, $I = 0$ (case of flux focussing, see Fig. 1 top right and Fig. 2 top) for ideal screening $\Lambda = 0$ (top) and for $\Lambda/a = 0.01$ (bottom) (60×60 grid points, only half the square is shown). Note that even such small Λ strongly changes $H_z(x, y)$ inside the superconductor, which penetrates much farther than Λ . The corresponding profiles $H_z(x, 0)$ are shown in Fig. 5.

the 3D magnetic stray field outside the film would be a formidable task. Fortunately, a much simpler calculation is possible using our above results and the known Lorentz force $\Phi_0 \nabla g(\mathbf{r})$ on the vortex: In a thought experiment, we move a first vortex from the film edge to its final position \mathbf{r}_i . At the edge the energy of this vortex, and also the interaction with other vortices needed later, are zero. Then its energy increases according to the integrated Lorentz force that originates from the interaction of this vortex with its own sheet current (more precisely: with the film edges, or with its images if an image method can be used, but this argument will not be required here). When the vortex has reached position \mathbf{r}_i its energy is just its self energy $F_s(\mathbf{r}_i)$. Now move a second vortex from the edge and merge it with the first one. The self energy of this new vortex, $4F_s(\mathbf{r}_i)$, is composed

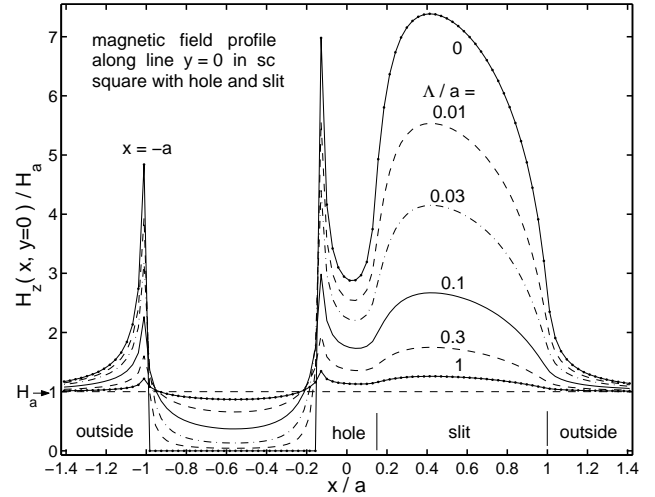


FIG. 5: The profiles of the magnetic field $H_z(x, 0)$ in the thin square of Fig. 1 (top right) taken along the x axis that passes through the hole and slit, in units of the applied field H_a and shown for several values of the 2D magnetic penetration depth $\Lambda = \lambda^2/d = 0, 0.01, 0.03, 0.1, 0.3$, and 1 in units of the half width a of the square. Same case as in Fig. 4 but with more grid points (100×100). Note that in the center of the square hole the magnetic field is enhanced by a factor of 3 when $\Lambda = 0$, $H_z(0, 0) \approx 3H_a$ (flux focussing); in the narrow slit $H_z(0.4a, 0) = 7.4H_a$ is even higher. Finite Λ reduces this enhancement and the spatial variation of $H(x, 0)$.

of the two self energies and the energy needed to move the second vortex against the sheet current of the first one, equal to the interaction energy V_{ii} , Eq. (29). From this we obtain the self energy $F_s(\mathbf{r}_i) = V_{ii}/(4 - 2) = \frac{1}{2}V_{ii}$ used in Eq. (30).

This result is exact within our numerical method, but in real films the self energy depends on the logarithm of the vortex core radius $\approx \xi$, the coherence length. In our numerics ξ is effectively replaced by some cut-off length of the order of the grid spacing. If required, an improved consideration of the vortex core is possible if its radius exceeds the local grid spacing. The core shape may then be taken from the GL solution for infinite films.¹⁷ If ξ is smaller than the grid spacing, the correct self energy is slightly larger than $\frac{1}{2}V_{ii}$, by a position-independent constant.

H. The fluxoid in films

The fluxoid Φ_f inside a given closed path S inside the film is defined as the magnetic flux through this loop plus the 2D penetration depth Λ times the path integral of the sheet current, $\Phi_f/\mu_0 = \int_S dx dy H_z(x, y) + \Lambda \oint d\mathbf{S} \mathbf{J}(x, y)$. When $g(x, y)$ and $H_z(x, y)$ are given on a rectangular grid, the integration path is conveniently chosen along a closed rectangle which runs in the middle between the grid points (App. A). The components J_x and J_y are then obtained from the difference of the values of $g(x, y)$

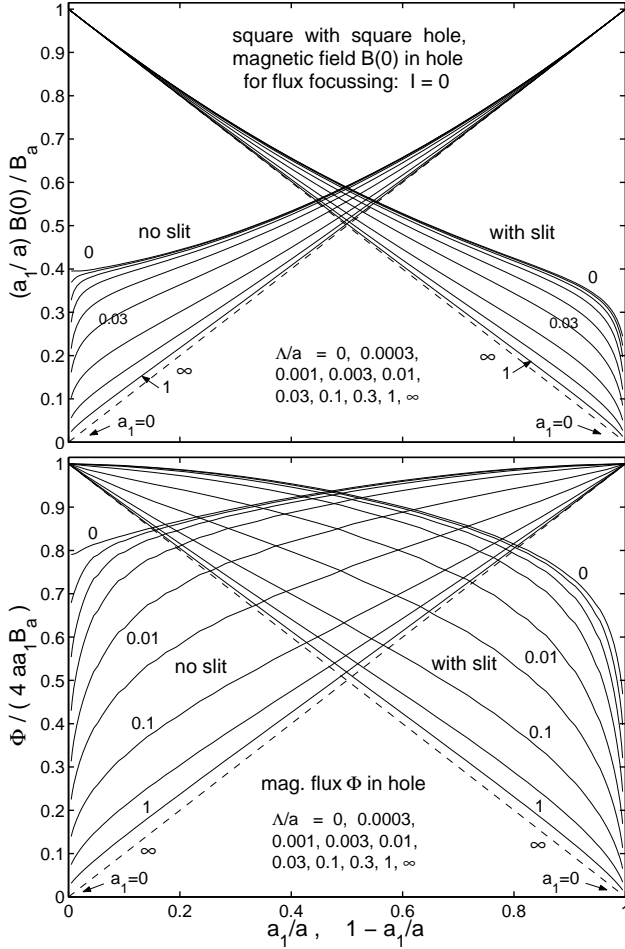


FIG. 6: Thin superconducting square (half width a) with central square hole (half width a_1) in applied field $B_a = \mu_0 H_a > 0$ and with no circulating current ($I = 0$, case of flux focussing). Plotted are the magnetic field $B(0) = \mu_0 H_z(0, 0)$ in the center of the hole (top) and the magnetic flux Φ inside the hole (bottom), for squares without slit (left, versus a_1/a) and with a narrow radial slit (right, versus $1 - a_1/a$), like in Fig. 1, for several values of the 2D penetration depths $\Lambda/a = 0 \dots \infty$. For $\Lambda = 0$ and $a_1/a \rightarrow 0$, both the minimum field and the average field in the hole diverge, $2B(0)/B_a \approx \Phi/4a_1^2 B_a \approx 0.80a/a_1$, see also the corresponding Figs. 15 and 16 of Ref. 4 for rings. For small holes, $a_1 \ll a$, the presence of a slit reduces this field enhancement.

at neighboring grid points, while the flux is the sum of $w_k H_z(x_k, y_k)$ over all points k inside this loop (App. A). The fluxoid obtained in this way from our solutions is indeed independent of the chosen path to within 4 to 5 significant digits, confirming thus that the solutions $g(x, y)$ and $H_z(x, y)$ are accurate also for finite Λ and even when $\Lambda \ll a$, see Figs. 7 and 8 below. Surprisingly, the obtained Λ -dependent g and H_z are quite accurate even when Λ is much smaller than the spacing of the numerical grid (typically $\geq a/50$), down to $\Lambda/a = 10^{-4}$. Besides this, the solutions for $\Lambda = 0$ are very accurate, with $H_z = 0$ inside the film, see Fig. 5.

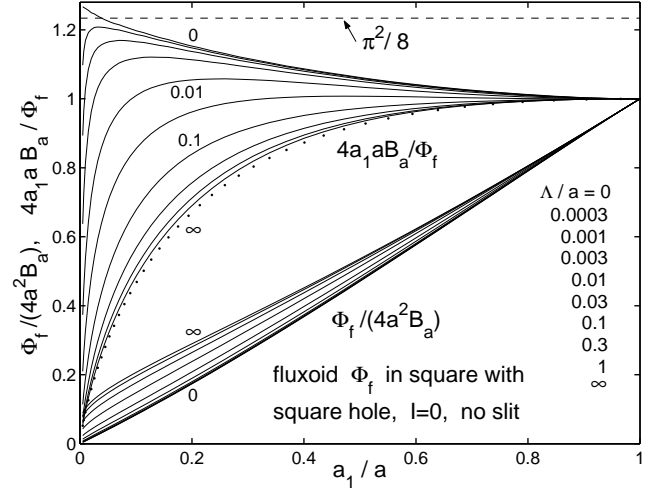


FIG. 7: The fluxoid Φ_f trapped in the square hole of a thin square without radial slit in the flux-focussing case of Fig. 6. This figure is very similar to Fig. 14 of Ref. 4 for rings. For small and large Λ nearly the same limiting curves are reached as for rings. The dots show the large- Λ limit for rings with radii a_1 and a : $4a_1 a B_a / \Phi_f \approx 2a_1 a \ln(a/a_1)/(a^2 - a_1^2)$.⁴ For $\Lambda = 0$ this Φ_f coincides with the Φ in Fig. 6 (bottom left).

III. EXAMPLE: FLUX FOCUSING

To illustrate how this method works and to check previous approximations of a slitted ring by a full ring,^{3,4} I discuss here the case of flux focussing in some detail. Consider a thin square film of half width a with a central square hole of half width a_1 ($a_1 \leq |x| \leq a$, $a_1 \leq |y| \leq a$) without slit, or with a narrow radial slit of width $\Delta \ll a$ extending along the x axis from $x = a_1$ to $x = a$ (Fig. 1). The current I circulating around the hole is forced to zero either “artificially” by putting the stream function $g(x, y) = 0$ everywhere outside the superconducting film, i.e., also in the hole and slit, or, naturally, by cutting a slit that makes $I = 0$. A uniform magnetic field $B_a = \mu_0 H_a$ applied along z is screened inside the film (or partly screened if the 2D penetration depth is $\Lambda = \lambda^2/d > 0$ for thickness $d < \lambda$) by a sheet current $\mathbf{J} = -\hat{\mathbf{z}} \times \nabla g = \nabla \times (\hat{\mathbf{z}}g) = (\partial g/\partial y, -\partial g/\partial x)$ that circulates clockwise near the edges and anticlockwise near the hole, see Fig. 1 (top right). This screening current causes a magnetic field in the hole (and in the slit) that can be much higher than H_a , see Figs. 4 and 5.

This field enhancement (or flux focussing) is plotted versus the relative hole size a_1/a in Fig. 6. For squares with no slit our numerics yields for small holes with $a_1/a \ll 1$ and ideal screening ($\Lambda = 0$) for the central field $B(0) = \mu_0 H_z(0, 0) \approx 0.40 B_a a/a_1$, and for the magnetic flux in the hole $\Phi \approx 0.80(4a_1^2 B_a) a/a_1$, i.e., both values diverge as $1/a_1$ when $a_1 \rightarrow 0$. This result is very similar to the flux focussing in circular rings depicted in Figs. 15 and 16 of Ref. 4. In particular, compared to a ring with radius a and hole radius a_1 , the limit $\Lambda = 0$

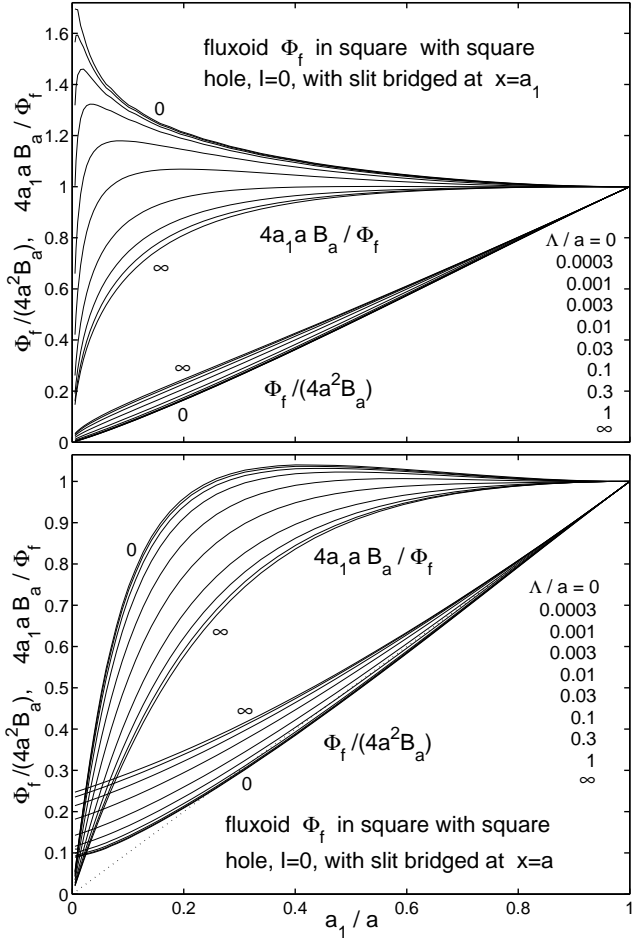


FIG. 8: The fluxoid Φ_f trapped in the square hole of the square of Fig. 7, but now with a narrow radial slit. Since the integration path of the fluxoid must run inside the superconductor, the path has to cross the slit by a narrow bridge, through which no current flows since $I = 0$ in this flux-focussing case. The plot shows the fluxoid when this bridge is chosen at $x = a_1$ (where the slit enters the hole, top) and at $x = a$ (where the slit exits the square, bottom). For large holes these two Φ_f are similar, but for small holes the larger integration path (bottom) yields a larger fluxoid since the integration includes the not negligible magnetic flux inside the narrow slit. For $\Lambda = 0$ the fluxoid of the smaller path (top) coincides with the flux Φ of Fig. 6 (bottom right).

(where the flux Φ equals the fluxoid Φ_f) is almost identical both for $B(0)/B_a$ and for the trapped flux plotted as the effective area $A_{\text{eff}} = \Phi_f/B_a$ referred to the hole area. Namely, for small holes at $\Lambda = 0$ one has for squares $A_{\text{eff}}/4a_1^2 \approx 0.80a/a_1$ and for circular rings $A_{\text{eff}}/\pi a_1^2 = (8/\pi^2)a/a_1 = 0.81a/a_1$ (exact result^{3,4,18}).

The corresponding results for the fluxoid Φ_f in squares without slit are shown in Fig. 7. As expected, Φ_f is independent of the integration path around the hole, which was chosen as any concentric square of half width between a_1 and a . Again, these Φ_f are very similar to those for circular rings shown in Fig. 14 of Ref. 4. For $\Lambda = 0$

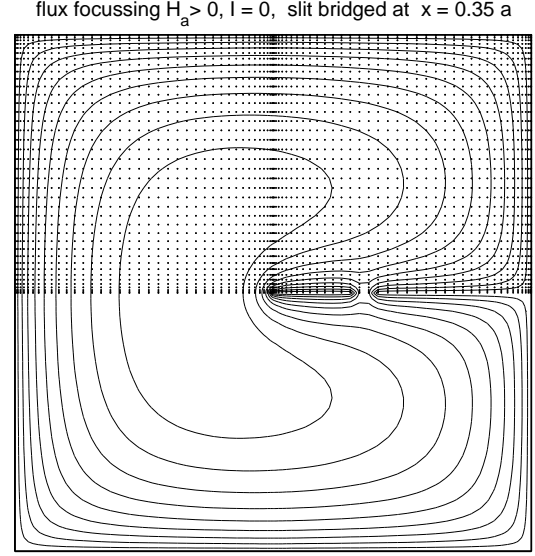


FIG. 9: The current stream lines in a thin superconductor square ($|x| \leq a$, $|y| \leq a$) with radial slit running at $y = 0$ from $x = 0$ to $x = a$, with a superconducting bridge at $x = a_2 = 0.35a$. Shown is the flux-focussing case $H_a > 0$, $I = 0$, i.e., no current crosses the bridge. $\Lambda/a = 0.01$. The dots mark the numerical grid of 80×80 points used for this plot.

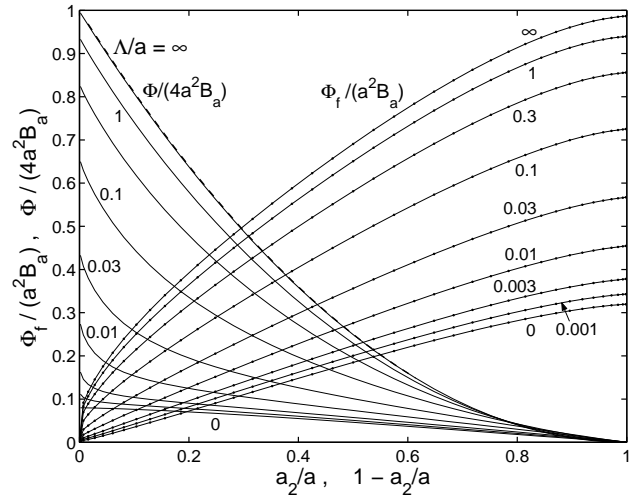


FIG. 10: The fluxoid Φ_f and magnetic flux Φ inside a concentric square of half width a_2 passing through the bridge (at $x = a_2$) of the slitted square of Fig. 9, plotted versus a_2/a for several values Λ/a . For better presentation Φ_f is shown 4 times larger than Φ , and Φ is plotted versus $1 - a_2/a$. For $\Lambda = 0$ one has $\Phi_f = \Phi$. For $\Lambda/a \gg 1$ one has $\Phi = 4a_2^2B_a$ (dashed line, full penetration), and $\Phi_f \approx (a_2/a)^{0.6}a^2B_a$.

(where $\Phi_f = \Phi$) they agree closely, as discussed above. But even for large $\Lambda \gg a$ and all hole sizes one has for rings⁴ $A_{\text{eff}} = 2(a^2 - a_1^2)/\ln(a/a_1)$, which is also a good approximation for the square, see the dots in Fig. 7.

Our 2D method allows us to check this approximation of slit-free flux focussing by considering squares or rings with slit. The results for the square with slit are depicted

in Fig. 6 [$B(0)$ and Φ plotted versus $1 - a_1/a$] and Fig. 8 (Φ_f for two different integration paths). One can see that for large holes these realistic $B(0)$, Φ , and Φ_f are similar to those of slit-free squares. However, for small holes $a_1/a \leq 0.2$, the field enhancement is considerably weakened by the presence of a slit, in particular for small Λ/a . For $\Lambda = 0$ the enhancement factor does no longer diverge as $1/a_1$ but tends to saturate (or possibly diverges very weakly, as one over some logarithm, as is the case for finite Λ in the absence of a slit). This means that the slit changes the screening currents near small holes considerably and thus reduces the field enhancement. As can be seen from the curves in Fig. 6, the presence of a slit has qualitatively the same effect as an increased value of Λ . This finding applies even though the width Δ of our slit was very small, $\Delta/a \approx 1/500$ and less.

By the same token, the presence of a slit changes the fluxoid Φ_f , Fig. 8. Moreover, the fluxoid now depends on the integration path. Since this path has to run inside the superconductor, one has to bridge the slit by a narrow superconducting bridge. The current through this bridge by definition is $I = 0$ in this flux-focussing case. It turns out that the resulting Φ_f depends on the position of this bridge. In Fig. 8 the two extreme cases are shown when this bridge is chosen at $x = a_1$ (where the slit emerges from the hole) and at $x = a$ (where the slit exits the square). For large holes these two choices yield similar Φ_f , but for small holes the large integration path yields a larger fluxoid than the small path.

One reason for this difference is that the fluxoid for the large path includes the magnetic flux Φ^{slit} inside the slit. For $\Lambda = 0$ one can show that Φ^{slit} is *very large* and almost does not decrease when the slit width Δ is decreased. From the simplified model of two long parallel strips (length $l \gg 2a$) with borders at $y = \pm a$ and $y = \pm \Delta/2$ in perpendicular field B_a , one finds for narrow slits the trapped flux^{7,19}

$$\Phi^{\text{slit}} = \pi a l B_a / \ln(8a/\Delta) \quad \text{for } \Delta \ll a. \quad (31)$$

For our squares with small hole we put the slit length $l \approx a$ and estimate the flux in the slit as $\Phi^{\text{slit}} = \pi a^2 B_a / \ln(8a/\Delta)$, which depends weakly on the slit width Δ . Comparing this with the flux in small holes from above, $\Phi^{\text{hole}} = (8/\pi)a_1 a B_a$, we get the ratio

$$\frac{\Phi^{\text{slit}}}{\Phi^{\text{hole}}} = \frac{\pi^2}{8 \ln(8a/\Delta)} \frac{a}{a_1} \approx 0.15 \frac{a}{a_1} \quad (32)$$

when Δ/a is of the order $1/500$. This means, for small holes with relative width $a_1/a < 0.15$, the magnetic flux even in a very narrow slit *exceeds* the flux in the hole. This finding explains why for small holes our flux-focussing results for slit-free and slitted disks differ considerably while they agree for large holes.

To check this further, we computed the magnetic flux Φ and the fluxoid Φ_f for a square with no hole, but with a narrow radial slit ranging from $x = 0$ to $x = a$ on the x axis. We bridge this slit by a narrow superconducting bridge centered at $x = a_2$, $0 < a_2 < a$, see Fig. 9.

The contour within which Φ and Φ_f are calculated is a concentric square passing through this bridge at $x = a_2$. We consider the case of flux-focussing ($H_a > 0$, $I = 0$), thus the current through the bridge is zero. In Fig. 10 the resulting Φ and Φ_f are plotted versus a_2/a for $\Lambda/a = 0, 0.001, 0.003, 0.01, 0.03, 0.1, 0.3, 1$, and ∞ . Note that the scales differ by a factor of 4. As expected, for $\Lambda = 0$ (ideal screening) one has $\Phi_f = \Phi$, and for $\Lambda/a \gg 1$ (full penetration) $\Phi = 4a_2^2 B_a$. Interestingly, For $\Lambda/a \ll 1$, one has approximately $\Phi_f \approx \Phi \approx (ca_2/a)4a^2 B_a$, where the constant $c \approx 0.08$ slightly depends on the slit width. This proportionality of the flux to the slit length within the square path, confirms that the magnetic flux in the narrow slit is approximately proportional to its length, and that Eq. (31) (derived for a long double strip) is a good approximation for our radial slit in the square.

IV. CONCLUSION

In this paper I presented a method that allows to calculate the 2D distributions of the sheet current $\mathbf{J}(x, y)$ and magnetic field component $H_z(x, y)$ (and, of course, the full 3D magnetic field) for thin flat superconductors of arbitrary shape. If the film thickness is $d < \lambda$ (the London depth), our method accounts for the 2D magnetic penetration depth $\Lambda = \lambda^2/d$, which may have any value, $0 \leq \Lambda < \infty$. The sheet current is expressed by the scalar potential (or stream function) $g(x, y)$, for which we list 10 useful properties in Sec. II A. The statics and dynamics of superconductors in the Meissner state, or with pinned and depinning vortices described by a complex or nonlinear resistivity, can be calculated. It is shown how this is generalized to multiply connected film shapes, e.g., squares or disks with a hole or closed slot, or with several such holes, slots, slits. For individual 2D vortices in the film we give their mutual interaction and self energy, which both depend on the specimen shape. The coupling of part of the magnetic flux of a moving vortex into a hole or slit is expressed in terms of the stream function $g(x, y)$, which is computed and depicted for some basic examples.

If a slitted square or circular disk is used as a SQUID, the applied magnetic field and applied currents induce a signal across the weak link that bridges the slit, and the moving vortices cause a noisy signal.¹ The SQUID signal in principle can be calculated by our 2D method, see Ref. 7 for a detailed theory of such SQUIDS and for the 1D problem of a long double strip that models a linear SQUID.

As a useful example for application of our 2D method we consider in Sec. III the phenomenon of flux focussing, which occurs when the total current circulating in a square or circular disk around a central hole is zero, $I = 0$. We compare the ‘‘ideal case’’ when the disk has no slit ($I = 0$ can then be achieved by appropriate magnetic history) with the realistic situation where a radial slit forces $I = 0$. We find good agreement for large holes,

but for squares with small central hole and radial slit, flux focussing is reduced by this slit. More applications will be published.

Acknowledgments

Helpful discussions with J. R. Clem, D. Koelle, G. P. Mikitik, Rinke Wijngaarden, and E. Zeldov are gratefully acknowledged. This work was supported in part by the German Israeli Research Grant Agreement (GIF) No G-705-50.14/01.

APPENDIX A: NUMERICAL TRICKS

For the computation of the stream function $g(\mathbf{r}) = g(x, y)$ with symmetry $g(x, -y) = g(x, y)$, $-a \leq x \leq a$, $0 \leq y \leq b$, a 2D grid of n points $\mathbf{r}_k = (x_k, y_k)$ with weights w_k , $k = 1 \dots n$, is chosen that covers the basic area $2a \times b$ (upper half of the rectangular film $2a \times 2b$). For simplicity we chose a rectangular grid $\mathbf{r}_{ij} = (x_i, y_j)$ with $i = 1 \dots 2n_x$ and $j = 1 \dots n_y$, e.g., the equidistant grid $x_i = -a + (i - \frac{1}{2})a/n_x$, $y_j = (j - \frac{1}{2})b/n_y$ with constant weights $w = 2ab/n$, $n = 2n_x n_y$. A better choice is a nonequidistant grid that is denser near the edges of the thin film. For example, for a rectangular film with rectangular hole with borders at $x = \pm a_1$, $y = \pm b_1$ and a narrow slit along $y = 0$ (see Fig. 1), a possible choice for the y_j and weights w_{yj} (and correspondingly for the x_i and w_{xi}) is $y_j = b_1 f(v_j)$, $w_{yj} = b_1 f'(v_j)/n_{y1}$, $v_j = (j - \frac{1}{2})/n_{y1}$ for $j = 1 \dots n_{y1}$, and $y_j = b_1 + (b - b_1)f(v_j)$, $w_{yj} = (b - b_1)f'(v_j)/(n_y - n_{y1})$, $v_j = (j - n_{y1} - \frac{1}{2})/(n_y - n_{y1})$ for $j = n_{y1} + 1 \dots n_y$, with any function $f(v)$ defined in $0 \leq v \leq 1$ and having a derivative $f'(v) = df/dv$ that at $v = 0$ and $v = 1$ is zero or small. We choose, e.g.,

$$\begin{aligned} f(v) &= (3v^2 - 2v^3)c + (1 - c)v, \\ f'(v) &= 6v(1 - v)c + 1 - c, \end{aligned} \quad (\text{A1})$$

with $0 \leq c \leq 1$; $c = 0$ means equidistant y_j with constant weights w_{yj} , and $c = 1$ (highest accuracy) means that the distances $y_{j+1} - y_j$ and weights w_{yj} vanish linearly at $y = 0$, $y = b_1$, and $y = b$. One can show that $\sum_j w_{yj} \varphi(y_j) \approx \int_0^b \varphi(y) dy$ for any sufficiently smooth function $\varphi(y)$.

For our 2D grid $\mathbf{r}_{ij} = (x_i, y_j)$ the weights are $w_{ij} = w_{xi} w_{yj}$. This 2D counting of grid points is required for

graphics and for computing derivatives, e.g., $\partial g(x, y)/\partial x$ and $\partial^2 g(x, y)/\partial x^2$. However, for computation of 2D integrals or for matrix operations, a 1D counting of the grid points is required: $\mathbf{r}_{ij} = \mathbf{r}_k = (x_k, y_k)$, $w_{ij} = w_k$, $k = i + 2n_x(j - 1) = 1 \dots n$, $n = 2n_x n_y$, and any 2D function like $g(x, y)$ is represented as a vector $g_k = g(x_k, y_k)$. The magnetic moment of the film, Sec. 2A, is then $m = \int g(\mathbf{r}) d^2 r \approx \sum_k g_k w_k$.

The magnetic flux through a closed rectangular path running between the grid points (along x and y values obtained from the above formulae for x_i , y_i by using half-integer values for i , j , e.g., $j = 7/2$) is then $\Phi = \mu_0 \sum'_k w_k H_z(x_k, y_k)$ where the sum is over all points k inside this loop.

Particular attention requires the computation of the Laplacian ∇^2 acting on $g(x, y)$ [e.g., in Eq. (13)], and computed by multiplication by a matrix ∇_{kl}^2 [e.g., in Eq. (15)]. This operator should contain the information that $g(x, y) = 0$ outside and on the outer edges of the rectangular film $|x| \leq a$, $|y| \leq b$, and that at $y = 0$ one has $\partial g(x, y)/\partial y = 0$ due to the symmetry $g(x, -y) = g(x, y)$. A 2D method that in principle applies to any 2D grid $\mathbf{r}_k = (x_k, y_k)$ computes ∇_{kl}^2 as the inverse of the Green function $G(\mathbf{r}, \mathbf{r}')$ satisfying $\nabla^2 G(\mathbf{r}, \mathbf{r}') = \delta(\mathbf{r} - \mathbf{r}')$ and the conditions that $G(\mathbf{r}, \mathbf{r}') = 0$ for \mathbf{r} on the outer edge of the rectangle $2a \times 2b$ and having even symmetry with respect to y . This $G(\mathbf{r}, \mathbf{r}')$ may be expressed by an infinite sum, with alternating signs, of functions $\ln |\mathbf{r} - \mathbf{r}' - \mathbf{R}_{mn}|/(4\pi)$, where the \mathbf{R}_{mn} are the vectors of a rectangular lattice with spacings $4a$ and $2b$. The resulting matrix indeed works, however, it is less accurate (and takes much more computation time) than the simple 1D method of computing $\nabla^2 g = \partial^2 g/\partial x^2 + \partial^2 g/\partial y^2$ from $g(x_i, y_j)$ and the values $g(x_{i\pm 1}, y_{j\pm 1})$ at the four neighboring points. With our nonequidistant grid we need for this the formula for $f''(x_i) = \partial^2 f/\partial x^2$ at $x = x_i$. Writing $f(x_{i-1}) = f_-$, $f(x_i) = f_0$, $f(x_{i+1}) = f_+$, $h_1 = x_i - x_{i-1} > 0$, $h_2 = x_{i+1} - x_i > 0$, one has

$$f''(x_0) \approx f_- \frac{2/h_1}{h_1 + h_2} - f_0 \frac{2}{h_1 h_2} + f_+ \frac{2/h_2}{h_1 + h_2}. \quad (\text{A2})$$

The boundary and symmetry conditions for $g(x, y)$ allow to define the required values of g on the grid lines lying one grid spacing outside the basic area $-a \leq x \leq a$, $0 \leq y \leq b$: $x_0 = -2a + x_1$, $x_{n_x+1} = 2a - x_{n_x}$, $y_0 = y_{-1}$, $y_{n_y+1} = 2b - y_{n_y}$, $g(x_0, y_j) = g(x_{n_x+1}, y_j) = g(x_i, y_{n_y+1}) = 0$, $g(x_i, y_0) = g(x_i, y_1)$.

¹ D. Koelle, R. Kleiner, F. Ludwig, E. Dantsker, and John Clarke, Rev. Mod. Phys. **71**, 631 (1999).

² J. Pearl, Appl. Phys. Lett. **5**, 65 (1964).

³ A. A. Babaei Brojeny and J. R. Clem, Phys. Rev. B. **68**, 174514 (2003).

⁴ E. H. Brandt and J. R. Clem, Phys. Rev. B **69**, 184509

(2004).

⁵ E. H. Brandt, Phys. Rev. B. **52**, 15442 (1995).

⁶ E. H. Brandt, Phys. Rev. B **64**, 024505 (2001).

⁷ J. R. Clem and E. H. Brandt, unpublished.

⁸ M. M. Khapaev, M. Yu. Kuprianov, E. Goldobin, and M. Siegel, Supercond. Sci. Technol. **16**, 24 (2003); see also: G.

- Hildebrandt and H. Uhlmann, *IEEE Trans. Magn.* **32**, 690 (1996); M. M. Khapaev, *Supercond. Sci. Technol.* **10**, 389 (1997); M. M. Khapaev, *IEEE Trans. Microwave Theory and Technol.* **41**, 217 (2001).
- ⁹ V. G. Kogan, J. R. Clem, and R. G. Mints, *Phys. Rev. B* **69**, 064516 (2004).
- ¹⁰ L. R. E. Cabral and F. M. Peeters, *Phys. Rev. B* **70**, 214522 (2004).
- ¹¹ R. J. Wijngaarden, H. J. W. Spoelder, R. Surdeanu, R. Griessen, *Phys. Rev. B* **54**, 6742 (1996).
- ¹² R. J. Wijngaarden, K. Heck, H. J. W. Spoelder, R. Surdeanu, R. Griessen, *Phys. C* **295**, 177 (1998).
- ¹³ L. Prigozhin, *J. Computational Phys.* **144**, 180 (1998).
- ¹⁴ E. H. Brandt, *Phys. Lett.* **114A**, 51 (1985); E. H. Brandt, P. Esquinazi, and H. Neckel, *J. Low Temp. Phys.* **63**, 187 (1985).
- ¹⁵ E. H. Brandt, *J. de Physique, Colloque C8*, **31**, (1987).
- ¹⁶ E. H. Brandt, *Phys. Rev. B* **46**, 8628 (1992).
- ¹⁷ E. H. Brandt, *Phys. Rev. B* **71**, 014521 (2005).
- ¹⁸ M. B. Ketchen, W. J. Gallagher, A. W. Kleinsasser, S. Murphy, and J. R. Clem, in *SQUID '85, Superconducting Quantum Interference Devices and their Applications*, edited by H. D. Hahlbohm and H. Lübbig (de Gruyter, Berlin, 1985), p. 865.
- ¹⁹ G. P. Mikitik and E. H. Brandt, *Phys. Rev. B* **64**, 092502 (2001).